J Mater Sci (2009) 44:6117–6124
DOI 10.1007/s10853-009-3846-4

Fracture toughness of zirconia nanoparticle-filled dental composites

K. S. Chan · D. P. Nicolella · B. R. Furman · S. T. Wellinghoff · H. R. Rawls · S. E. Pratsinis

Received: 16 July 2009 / Accepted: 25 August 2009 / Published online: 10 September 2009

Abstract The fracture toughness of dental composites containing zirconia nanoparticles dispersed in a bisphenol A glycol dimethacrylate-based monomer blend (GTE) was studied for several yttria contents. Three-point bend test bars with and without a notch were tested at ambient temperature to determine elastic modulus, flexure strength, and fracture toughness. The ZrO_2 nanoparticles increased the fracture toughness of the nanocomposites compared to previous results for the matrix and Schott glass-filled nanocomposites. X-ray diffraction analyses revealed mostly tetragonal ZrO_2 in the nanocomposites before and after testing, in agreement with a theoretical analysis. The enhancement in fracture toughness in ZrO_2-filled nanocomposites was caused mainly by the higher values of particle toughness and interface toughness in GTE/ZrO_2 compared to those of GTE/Schott glass nanocomposites.

K. S. Chan (✉) · D. P. Nicolella · S. T. Wellinghoff
Southwest Research Institute®, San Antonio,
TX 78238, USA
e-mail: kchan@swri.edu

B. R. Furman · H. R. Rawls
University of Texas Health Science Center, San Antonio,
TX 78249, USA

S. E. Pratsinis
Particle Technology Laboratory, Department of Mechanical and Process Engineering, ETH Zurich, 8092 Zurich, Switzerland

Present Address:
B. R. Furman
Southwest Research Institute®, San Antonio,
TX 78238, USA

Introduction

There is interest in developing dental composites reinforced with nanosized particles with near-zero volumetric shrinkage during curing and highly translucent and radiopaque post curing [1–8]. Other desired properties of the nanocomposites include high strength, good fracture toughness, and excellent wear resistance [6]. Nanosized particles are attractive fillers for dental composites because they improve composite strength and wear resistance. On the other hand, it is not obvious that nanosized particles would enhance the fracture resistance of dental nanocomposites since fracture toughness usually scales with the ½ power of the characteristic microstructural length scale controlling the fracture process. To be an effective toughening agent, the nanosized particles must increase the process zone size at the onset of critical fracture either through an increase in the fracture strength, due to their small size scale, or the inducement of one or more new toughening mechanisms by virtue of their size scale or the large surface area-to-volume ratio.

An earlier study by the authors [9] demonstrated that the fracture toughness of dental composites can be enhanced using colloidal SiO_2 and 0.4-μm Schott glass fillers (a mixture of 50% SiO_2, 30% BaO, 10% Al_2O_3, and 10% B_2O_3 by weight; Schott glass GmbH, Landshut, Germany) in bisphenol A glycol dimethacrylate (bis-GMA)-based monomer blend (GTE) resin matrix, which is a 3-component monomer solution containing 37.5 wt% bis-GMA, 25 wt% triethylene glycol dimethacrylate (TEGDMA), and 37.5 wt% bisphenol A ethoxylate dimethacrylate (bis-EMA). The study [9] showed that the toughening ratio in these composites can be as high as 3. The dominant fracture mechanism was crack deflection by nanoparticles and interface crack propagation along the

matrix/particle interface. The sources of composite toughness enhancement were determined to be twofold: (1) interface crack growth around a particle lowers the near-tip effective stress intensity and increases the fracture toughness by about 30–60% of the matrix toughness and (2) interface toughness of matrix and silanized nanoparticles appears to be two to three times higher than that of the matrix toughness [9]. Nanosized particles improve the overall fracture toughness by enhancing the interface bonding between the particle and matrix through a higher surface area to volume ratio. Despite a threefold increase, the fracture toughness values of the nanocomposites, which is in the range of 0.4–0.8 $MPa(m)^{1/2}$, are still low and need further improvement. On the other hand, a theoretical analysis [9] indicates that further increase in the interface toughness of GTE/SiO_2 and GTE/Schott glass nanocomposites might cause a change of the dominant fracture mechanism from interface fracture to particle fracture as the interface toughness approaches that of the particles. As a result, both the interface toughness and the particle toughness must be increased to achieve higher fracture toughness in the nanocomposites.

The objective of this article is to report the results of an investigation to improve the fracture toughness of dental nanocomposites using nanosized ZrO_2 fillers in GTE matrix. Zirconia nanoparticles have been selected because of a relative high fracture toughness (2.6 $MPa(m)^{1/2}$ [10] compared to 1 $MPa(m)^{1/2}$ for SiO_2 and Schott glass [9]). Furthermore, nanosized spherical ZrO_2 particles exist in the tetragonal structure that can be induced to transform to the monoclinic structure under stress [11, 12], thereby providing the possibility of toughness enhancement via stress-induced transformation toughening [13, 14]. Since the tetragonal-to-monoclinic phase transformation results in a volume increase [11–14], nanosized ZrO_2 may also be utilized to reduce volumetric shrinkage during the curing of resin-based nanocomposites. In this article, we will first report the fabrication of the ZrO_2-filled nanocomposites, followed by the experimental procedures for performing the fracture toughness tests. Experimental results of the fracture tests will be presented together with the corresponding fracture and toughening mechanisms. The experimental results indicate that ZrO_2 nanoparticles enhance the fracture toughness of nanocomposites without undergoing a phase transformation. The experimental results will be compared against a theoretical analysis, which shows that the tetragonal ZrO_2 nanoparticles are stable at the particle size range examined. The increase in fracture toughness observed in ZrO_2-filled nanocomposites is caused mainly by a higher fracture toughness of tetragonal ZrO_2 compared to that of the Schott glass nanoparticles.

Experimental methods

Composite resins were formulated with a 3-component monomer solution (GTE) containing 37.5 wt% bis-GMA, 37.5 wt% bis-EMA, and 25 wt% TEGDMA (Esschem Inc., Linwood, PA). A liquid photoinitiator system comprising camphorquinone and dimethylaminoethyl methacrylate (0.4 g:1.0 g) was added to the monomer solution at a total level of 3% (w/w) prior to formulation with fillers. ZrO_2 nanoparticles with an average particle size of about 12 nm, with and without yttria dopant, were selected for this study. Pure ZrO_2 nanoparticles were fabricated (ETH, Zurich, Switzerland) at 100 g/h by flame spray pyrolysis (FSP) of zirconium propoxide in ethanol solutions [15]. Yttria-doped zirconia nanoparticles (1–10 mol%) were made (ETH, Zurich, Switzerland) also at about 100 g/h by FSP of yttrium hexahydrate and zirconium carbonate hydroxide oxide ($(Zr(OH)_2(CO3)_2{\cdot}ZrO_2$ = ZC, ZrO_2 content ~44.4 wt%, LUUnited Int'l Inc.) in acetic acid (Fluka, 99.8% AcOH), 2-ethylhexanoic acid (2-EHA, Fluka, 99%), and EtOH solutions as described by Jossen et al. [16]. The particle size and the crystal structure were determined by X-ray diffraction (XRD) (Bruker Instruments, Model D8, Billercia, MA) and nitrogen adsorption (BET), using the procedure described earlier [15, 16]. The resolution of the XRD was 1% yttria. Yttria formed a solid solution with the zirconia, and no separate yttria phases were present, regardless of the yttria-stabilized zirconia synthesis conditions, up to 10% yttria content [16].

To fabricate the nanocomposites, ZrO_2 particles were suspended by sonication in acetonitrile and surface treated by the addition of either diethyl (vinyl)phosphonate or diethyl(methacryloylmethyl)phosphonate. Particles were exchanged into the dental resin by centrifugation and redispersion (wet) into dichloromethane, followed by addition of the resin monomer and evaporation of the volatiles. Rectangular bar specimens 27.5 mm in length and 2 mm × 2 mm in cross-section were fabricated by casting the composite resins into a glass mold. The specimens were pre-cured for 1 min, passing a handheld dental curing lamp (Optilux 400, Demetron Research Corp.) back and forth over the length of the specimen, to permit release from the mold. Post-curing was then performed in a halogen light box (CureLite Plus, Jeneric/Pentron, Inc.) for 10 min to assure maximum conversion of the resin.

The cured specimens were divided into two groups: (1) six flexure specimens for strength measurements and (2) six specimens for fracture toughness measurements. All six fracture toughness specimens of each composite were notched to about 0.5 mm depth at the mid span using a saw with a steel blade. Subsequently, a sharp crack was introduced at the notch tip by pressing a razor blade at the root region. Figure 1 shows a sharp crack induced at the notch

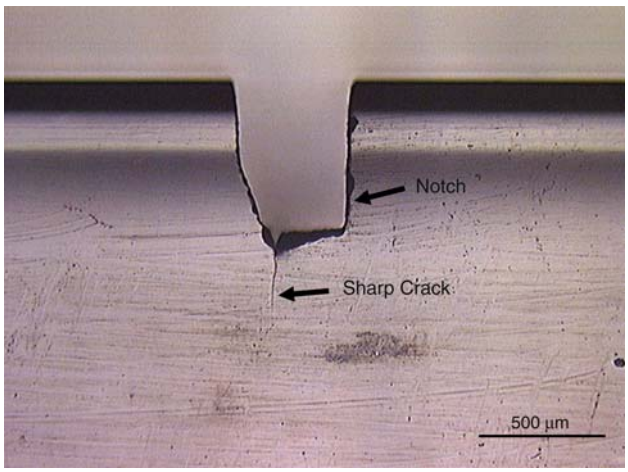

Fig. 1 Three-point bend specimen of GTE/ZrO_2 nanocomposite with a sharp crack induced by pressing a razor blade at the notch root

root of the nanocomposites using this method. The notch tip was not controlled or measured since the induced crack tip was sharp, as shown in Fig. 1. The total crack length was measured as the sum of the notch length and the length of the sharp crack initiated from the notch.

Three-point bend tests were conducted under a displacement rate of 1 mm/min in screw-driven loading machine (Sintech, Eden Prairie, MN). Unnotched specimens were tested for elastic modulus and flexure strength, and the notched and precracked specimens were tested for fracture toughness. Six flexure specimens and six cracked specimens ($n = 6$) were tested for each of the nanocomposites to determine the flexure strength and fracture toughness, respectively. Linear load–displacement curves were obtained for both the flexure tests and the fracture toughness tests. After testing, XRD analysis was performed (Kristalloflex 850, Siemen AG, Karlsruhe, Germany) on the center portions of the test specimens near the fracture surfaces and the outer unloaded regions to determine the crystal structure of the ZrO_2 nanoparticles. The microstructure of the nanocomposites was examined by atomic force microscopy (AFM; Dimension 3000, Veeco, Santa Barbara, CA). The fracture toughness values, K_{IC}, were computed on the basis of the crack length, and the maximum load at fracture according to the ASTM E399 procedure [17]. Data were analyzed by using one-way ANOVA and post hoc Tukey comparison tests.

Results

The characteristics of the ZrO_2 nanoparticles and the loading level of the nanocomposites before fabrication are summarized in Table 1. Nanocomposites 1–7 were loaded to 50 wt% fillers, while Nanocomposite 8 was loaded to 31 wt% fillers. These loading levels were selected because higher loadings were not possible to achieve without reduced workability and gelation of the uncured nanocomposite. Fumed-silica fillers of a similar size to the ZrO_2 nanoparticles are used at levels <10 wt% in hybrid dental composites. Thus, the chosen loadings are within a relevant range for the substitution of silica in these composites.

The microstructure of GTE/ZrO_2 nanocomposite without yttria addition is presented in Fig. 2a and b, which shows the ZrO_2 as light particles in a GTE matrix at two magnifications. Figure 2b shows that the dispersion of ZrO_2 in the GTE matrix is not uniform microscopically and the ZrO_2 particles are larger than 12 nm in diameter. These larger sizes suggest that there is some agglomeration or clumping of the 12-nm diameter particles and a concentration of particles in local regions. The agglomerate particle sizes were measured from AFM images taken randomly on specimen surfaces. The average agglomerate particle size and standard deviations for Nanocomposites 1, 3, 4, and 5 after fabrication are tabulated in Table 1. The agglomerate particle sizes in these four nanocomposites are

Table 1 A summary of the filler material, loading level, ZrO_2 particle size, and structure before and after composite fabrication

Nanocomposite	Filler material	Filler loading (wt%)	ZrO_2 initial size (nm)	Agglomerate ZrO_2 size in composite (nm)	ZrO_2 structure in composite
1 (Nano_1)	ZrO_2	50	12	16.7 (10.2)	Tetragonal[a]
2 (Nano_2)	ZrO_2 + 7 mol% SiO_2	50	12	–	Tetragonal
3 (Nano_3)	ZrO_2 + 2 mol% Y_2O_3	50	12	68.2 (21.6)	Tetragonal
4 (Nano_4)	ZrO_2 + 2.5 mol% Y_2O_3	50	12	78.8 (28.9)	Tetragonal
5 (Nano_5)	ZrO_2 + 1 mol% Y_2O_3	50	12	27.2 (10.8)	Tetragonal
6 (Nano_6)	ZrO_2 + 1.5 mol% Y_2O_3	50	12	–	Tetragonal
7 (Nano_7)	ZrO_2 + 10 mol% Y_2O_3	50	12	–	Cubic
8 (Nano_8)	ZrO_2 + 3 mol% Y_2O_3	31	12	–	Tetragonal

Values in parenthesis are standard deviation

[a] With small amounts of monoclinic ZrO_2

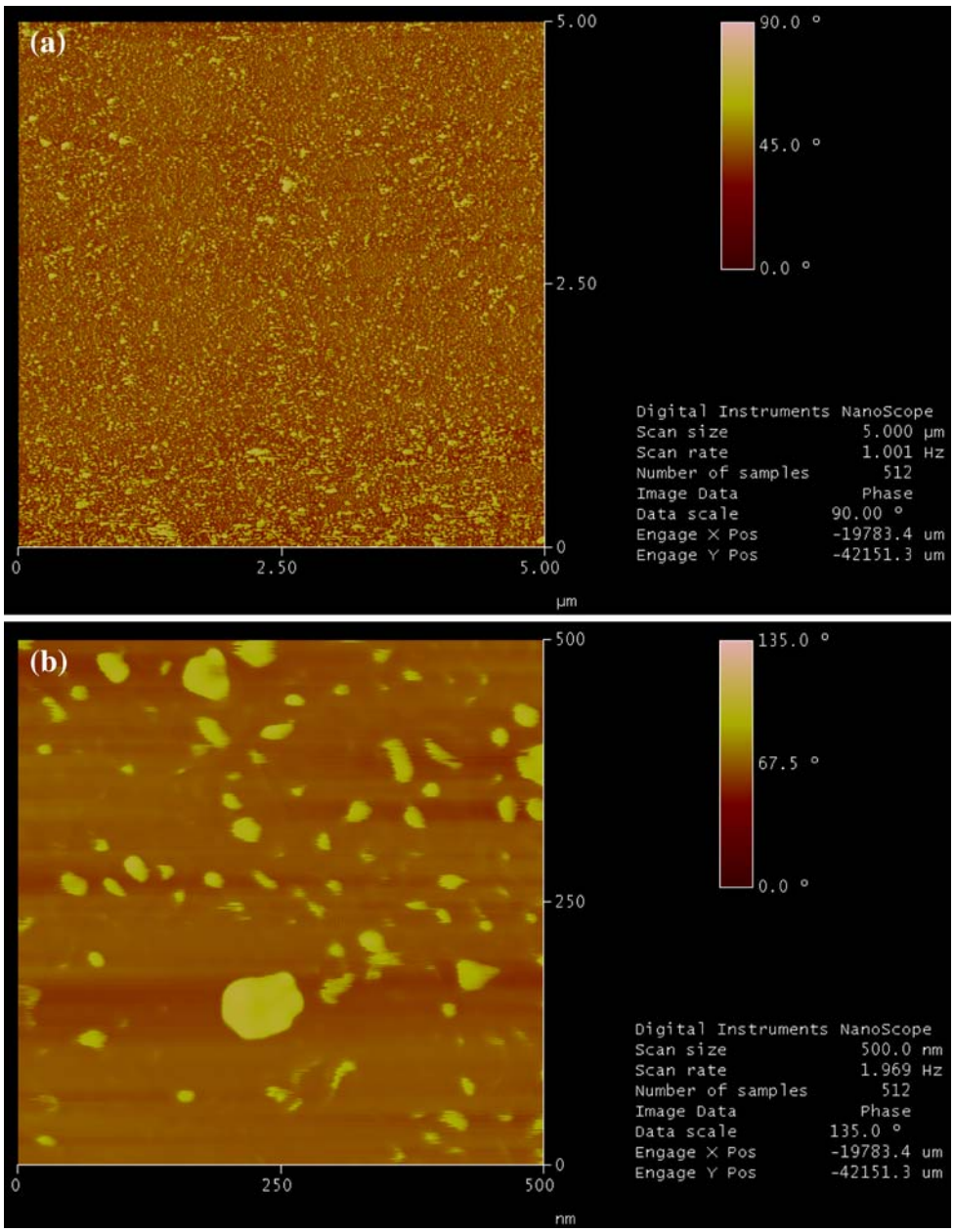

Fig. 2 Microstructures of GTE/ZrO_2 nanocomposites revealed by AFM: **a** 5 µm × 5 µm scan area. **b** 500 nm × 500 nm scan area. ZrO_2 particles are shown as *light* and the GTE matrix is *dark*

fitted by lognormal distributions ($p < 0.05$), which are compared in Fig. 3. In these four cases, the agglomerate sizes of the ZrO_2 particles in the nanocomposites were higher than the starting particle size (12 nm) due to agglomerations of particles during the composite fabrication process [8]. Neither the pure zirconia nor the yttria-doped zirconia nanoparticles were completely aggregated in the prepared composites, as determined by the close proximity of the XRD crystallite sizes to previously determined BET grain sizes [15, 16].

Results of the elastic modulus, flexure fracture strength, and fracture toughness of GTE/ZrO_2 nanocomposites are presented in Table 2. For comparison, Table 2 also presents the fracture toughness of the unfilled GTE resin and tetragonal ZrO_2 in bulk form and the commercial dental material Z100 (3M, Minneapolis, MN). The elastic modulus of the nanocomposites ranges from 3.74 to 4.4 MPa, while the flexure strength ranges from 71.3 to 106 MPa. For fracture toughness, the lowest value (0.55 $MPa(m)^{1/2}$) was observed in the ZrO_2 nanocomposite without yttria addition and the highest value (0.86 $MPa(m)^{1/2}$) was observed in ZrO_2 nanocomposites with 10% yttria. XRD results indicated that pure ZrO_2 particles or slightly doped ones with yttria (<3 mol%) were mostly tetragonal before [18] and after fracture tests for Nanocomposites 1–6. Typical results for Nanocomposite 4 before and after fracture testing are shown in Fig. 4a and b, respectively. Among these materials, monoclinic ZrO_2 in very small

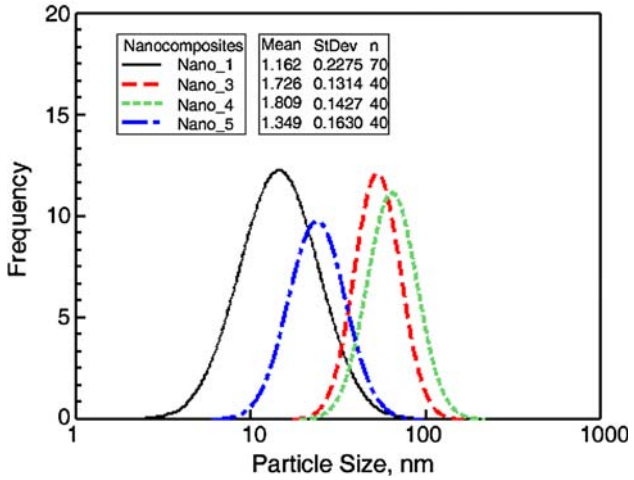

Fig. 3 Distributions of agglomerate ZrO_2 particle size in four ZrO_2/GTE nanocomposites

amounts were detected only in ZrO_2 nanocomposites without yttria addition (Nanocomposite 1). Nanocomposites 7 and 8 showed cubic ZrO_2 particles before and after fracture tests. In all cases, the ZrO_2-filled nanocomposites exhibit a statistically higher ($p < 0.05$) fracture toughness than Z100, which was used as a control, and the GTE resin.

The fracture mechanisms in the nanocomposites were identified by fractographic examination in a 3D digital microscope (Keyence, Model VHX-100, Woodcliff, NJ). At low magnifications (×1,000), the fracture surfaces in the nanocomposites were typically very flat. At higher magnifications (×4,000), the fracture surfaces exhibited numerous circular features that were about 1 μm in diameter and larger ones at 3–4 μm in diameter, as shown in Fig. 5a. A surface height map of these features, shown in

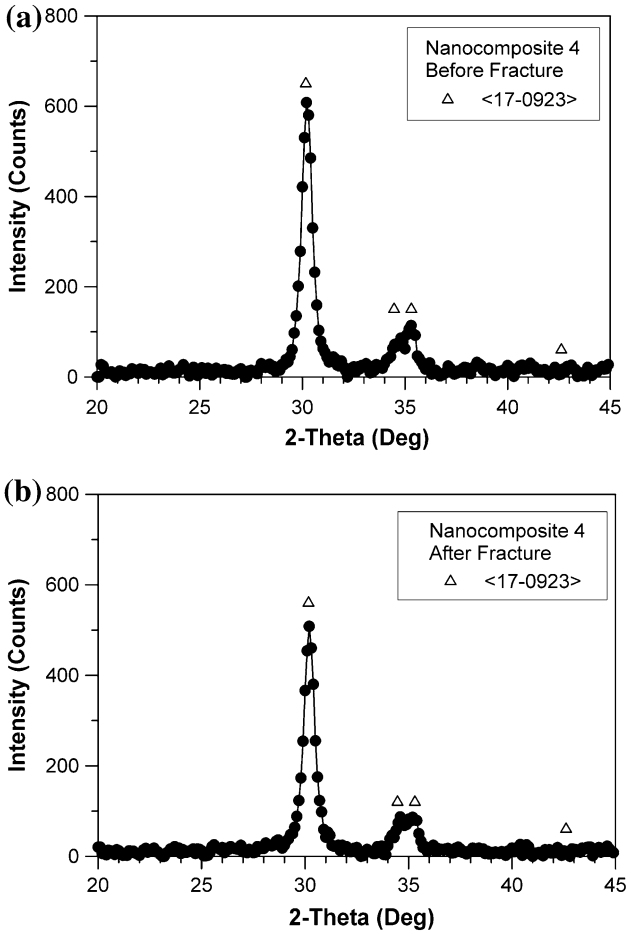

Fig. 4 X-ray diffraction results indicate the presence of tetragonal ZrO_2 (JCPDF card no. <17-093> [23]) in the nanocomposite before and after fracture testing: **a** Before fracture test. **b** After fracture test

Table 2 A summary of the elastic modulus, fracture stress, and fracture toughness of GTE/ZrO_2 nanocomposites

Nanocomposite	Filler material	Filler loading (wt%)	Elastic modulus (GPa)	Fracture stress (MPa)	Fracture toughness ($MPa(m)^{1/2}$)
1 (Nano_1)	ZrO_2	50	4.14 (0.18)	97.41 (12.9)	0.55 (0.08)
2 (Nano_2)	ZrO_2 + 7 mol% SiO_2	50	3.74 (0.20)	71.3 (25.5)	0.70 (0.18)
3 (Nano_3)	ZrO_2 + 2 mol% Y_2O_3	50	4.02 (0.38)	106.0 (10.8)	0.77 (0.11)
4 (Nano_4)	ZrO_2 + 2.5 mol% Y_2O_3	50	4.04 (0.16)	96.8 (22.8)	0.79 (0.17)
5 (Nano_5)	ZrO_2 + 1 mol% Y_2O_3	50	4.40 (0.26)	93.9 (17.0)	0.76 (0.11)
6 (Nano_6)	ZrO_2 + 1.5 mol% Y_2O_3	50	3.97 (0.25)	73.4 (33.0)	0.79 (0.12)
7 (Nano_7)	ZrO_2 + 10 mol% Y_2O_3	50	4.18 (0.15)	86.2 (16.8)	0.86 (0.12)
8 (Nano_8)	ZrO_2 + 3 mol% Y_2O_3	31	–	–	0.80 (0.17)
GTE resin	Unfilled	0	2.90 (0.14)	123.3 (4.02)	0.22 (0.06)
Z100	N.A.	N.A.	17.76 (3.44)	136.34 (32.90)	0.44 (0.08)
ZrO_2 [10, 11]	N.A.	N.A.	–	–	2.6 (0.52)

The ZrO_2-filled nanocomposites exhibit a statistically higher ($p < 0.05$) fracture toughness than the control (Z100) and the GTE resin
Values in parenthesis are standard deviation

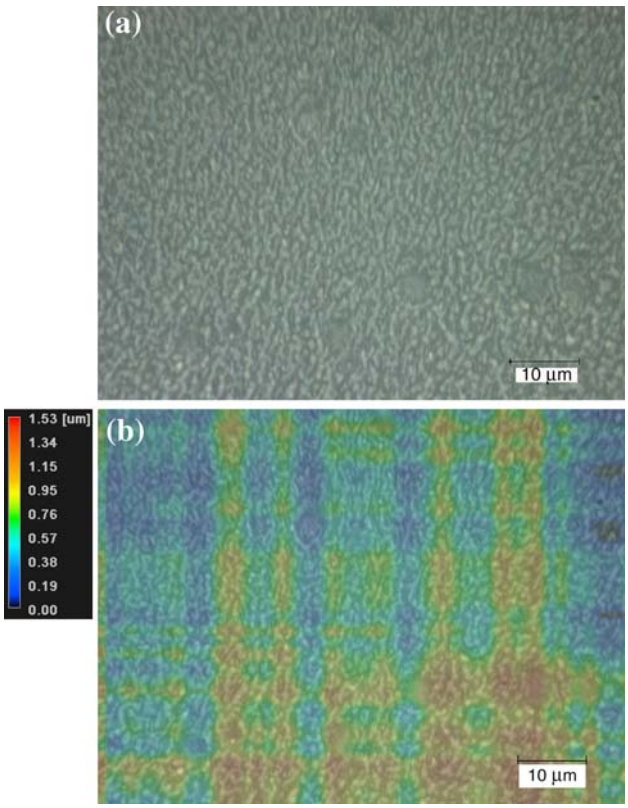

Fig. 5 3D digital images of the fracture surface of Nanocomposite 4 (Nano_4) showing: **a** Numerous circular features 1 µm in diameter and some circular features at 3–4 µm in diameter. **b** A surface height profile indicating the presence of hills (*light*) and valleys (*dark*) on the fracture surface. The hills correspond to particles sticking out on the surface, while the valleys (*dark*) indicate holes created by particles being pulled out from the fracture surface

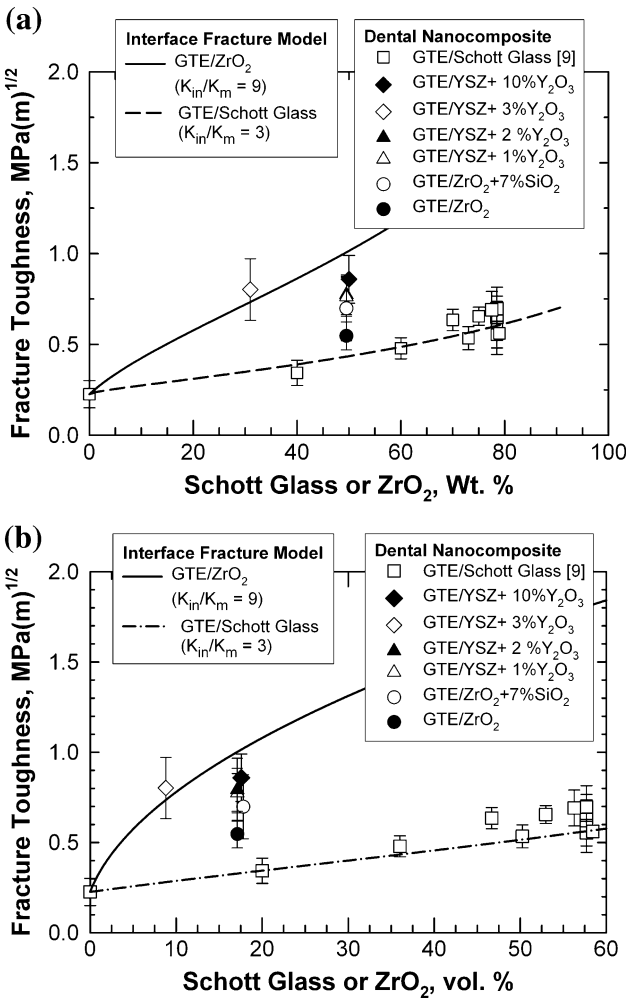

Fig. 6 Fracture toughness of GTE/ZrO_2 nanocomposites compared to GTE/Schott glass nanocomposites from Chan et al. [9]: **a** As a function of weight percent particles. **b** As a function of volume percent particles

Fig. 5b, indicated that some of the circular features were particles (light) sticking out on the surface, while others (dark) were holes or depressions. These observations suggested that based on their size, clumps of ZrO_2/GTE composite particles were pulled out from the fracture surfaces, creating holes (dark) on the fracture surface. On the same surface, individual clumps of composite particles (light) were visible on the fracture surface (Fig. 5b). Similar results were observed in other nanocomposites [9]. These results are consistent with the AFM observations that ZrO_2 nanoparticles often occur in clumps in the nanocomposites. However, the particles and voids observed on the fracture surfaces were at least ten times larger than the largest agglomerated particle sizes shown in Fig. 3. Thus, the observation suggests that the fracture mechanism involved crack deflection around clumps of ZrO_2 particles and pullout of composite clumps that contained both ZrO_2 agglomerate particles and the GTE matrix.

The fracture toughness data of GTE/ZrO_2 nanocomposites are compared against those of GTE/colloidal SiO_2/Schott glass from an earlier study [9] in Fig. 6, which shows the fracture toughness values as a function of volume fraction of the nanoparticles in the composites. The comparison indicates that ZrO_2-filled nanocomposites are more fracture resistant than those containing silica nanoparticles. For both types of composites, the fracture mechanisms are predominantly crack deflection by nanoparticles [9]. The higher fracture toughness observed in GTE/ZrO_2 nanocomposites appears to originate from crack deflection by the ZrO_2 fillers in a tortuous crack path around the clumps of particles and along the matrix/particle interface, as suggested by the fractographic observations in Fig. 5. For a deflected crack advancing on the particle/matrix interface, the fracture toughness of the nanocomposites arises from contributions of the matrix and interface toughness, and is given by [9, 19]

$$K_C = \left[1 + \alpha_{tl}\alpha_{pr}\left(\frac{K_{in}}{K_m}\right)^2\right]^{1/2} K_m \quad (1)$$

where K_{in} is the interface toughness, K_m is the fracture toughness of the matrix, α_{tl} is the toughness parameter for deflection of tilted cracks, and α_{pr} is the toughness parameter for crack deflection by an interface crack advancing from the pole and around spherical particles. The values of α_{tl} and α_{pr} are 0.87 and 1.6, respectively [9]. Using $K_m = 0.22$ MPa(m)$^{1/2}$ for the GTE resin matrix and assuming $K_{in}/K_m = 9$, Eq. 1 is applied to correlate the fracture toughness of GTE/ZrO_2 composites. The calculated curve (solid line) is compared against experimental data for GTE/ZrO_2 composites from this study. The comparison showed that $K_{in}/K_m = 9$ overpredicted the fracture toughness values of GTE/ZrO_2 nanocomposites at the 50% loading level, suggesting that the K_{in}/K_m value for these nanocomposites is <9. Figure 6 also shows a comparison of GTE/ZrO_2 results against those of GTE/Schott glass particles from a previous study [9]. For GTE/Schott glass particles, the increase in fracture toughness with increasing filler contents is well described by Eq. 1 using a K_{in}/K_m ratio of 3 and $K_m = 0.22$ MPa(m)$^{1/2}$, which is shown as the dashed line in Fig. 6. In contrast, the experimental data from GTE/ZrO_2 nanocomposites at the 50% loading level is above the dashed line ($K_{in}/K_m = 3$) but below the solid line ($K_{in}/K_m = 9$). The comparison of these two sets of experimental data and calculated curves revealed that the fracture toughness of GTE/ZrO_2 nanocomposites are higher than those of GTE/Schott glass at a given volume fraction or loading level of nanoparticles by virtue of a high K_{in}/K_m ratio ($3 \leq K_{in}/K_m \leq 9$) resulting from better interface bonding between the matrix and the nanoparticles. The fracture toughness (K_{IC}) of fully established cubic ZrO_2 determined by fracture mechanics specimens is 2.8 MPa(m)$^{1/2}$, while it ranges from 5 to 6.5 MPa(m)$^{1/2}$ for partially stabilized tetragonal ZrO_2 [20]. The higher fracture toughness values in the partially stabilized tetragonal ZrO_2 are due to the presence of transformation toughening during the fracture process. For tetragonal ZrO_2 in the absence of transformation toughness, the fracture toughness (K_{IC}) determined by the Vickers indentation method is 2.6 MPa(m)$^{1/2}$ [9], while it is 2.8 ± 0.14 MPa(m)$^{1/2}$ for cubic ZrO_2 [11]. A direct comparison [21] of Vickers indentation fracture toughness (K_{IV}) and standard fracture toughness (K_{IC}) determined using fracture mechanics specimens such as single-edge-notched beam and double cantilever beam indicated that the two methods produced comparable results within the ±20% experimental scatters. Thus, the fracture toughness of ZrO_2 particles is at least 2.6 ± 0.52 MPa(m)$^{1/2}$ and may be higher if transformation toughness occurs. In comparison, the fracture toughness of Schott glass particles is about 1 MPa(m)$^{1/2}$. The higher fracture toughness established by GTE/ZrO_2 nanocomposites can therefore be attributed to a higher fracture toughness of the ZrO_2 particles and a higher interface toughness or K_{in}/K_m ratio. It also appears that the higher fracture toughness of the ZrO_2 particles give rise to higher interface fracture toughness values (0.8–1.8 MPa(m)$^{1/2}$) and the corresponding ranges of the K_{in}/K_m ratio ($3 \leq K_{in}/K_m \leq 9$) so that the sizes of the pullout composite particles are more than ten times larger than the sizes of the agglomerate ZrO_2 particles.

Discussion

The results of this investigation clearly showed that the tetragonal ZrO_2 nanoparticles did not transform to the monoclinic structure during fracture testing. Thus, transformation toughening can be ruled out as a source of the toughness enhancement in the GTE/ZrO_2 nanocomposites. To understand the absence of transformation toughening in the ZrO_2-filled composites, the theoretical analysis by Suresh et al. [22] for stress-free transformation was modified to define the crystalline size and yttria content required for triggering the onset of stress-induced phase transformation in zirconia [11–14]. The theoretical model is a thermodynamic model that takes into account the free energy change associated with the transition of ZrO_2 from the tetragonal-to-monoclinic structure, the surface energy of the nanosized particles, the elastic strain energy, and the presence of an external stress [12–14]. For spherical particles, the critical particle diameter (d^*) for the transformation of tetragonal-to-monoclinic ZrO_2 is given by [22]

$$d^* = \frac{-10(\Delta h_{surf} - T\Delta S_{surf})}{\Delta H_{vol} - T\Delta S_{vol} - \sigma_c \theta^T} \quad (2)$$

where Δh_{surf} and ΔS_{surf} are the enthalpy and entropy change associated with the surface energy difference of the tetragonal-to-monoclinic transformation of nanosized ZrO_2, respectively; ΔH_{vol} and ΔS_{vol} are the enthalpy and entropy change associated with the volume free energy change of tetragonal-to-monoclinic transformation of infinitely sized ZrO_2, respectively; T is absolute temperature; σ_c is the transformation stress; and θ^T is the volume change associated with the tetragonal-to-monoclinic transformation. The $\sigma_c\theta^T$ term [11–14] accounts for the presence of stress during the phase transformation process.

Using the thermodynamic data [22] in the literature, the theoretical model was utilized to compute the critical crystalline size for the transition from tetragonal-to-monoclinic ZrO_2 as a function of yttria content. The transformation stress was taken to be 0 (stress-free transformation), 250, and 500 MPa and $\theta^T \approx 0.04$ [14]. The theoretical results are compared against experimental data [10, 11] and theoretical results of Suresh et al. [22] in

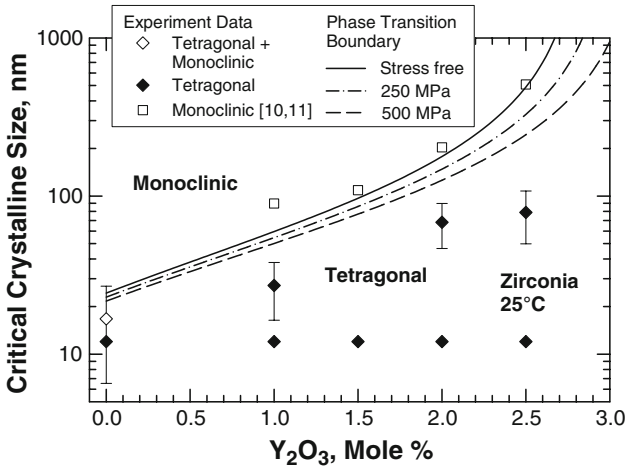

Fig. 7 Calculated critical crystalline ZrO_2 diameter for the tetragonal-to-monoclinic transformation at three stress levels as a function of yttria content compared to experimental data from the literature [10, 11] and this study

Fig. 7. Figure 7 shows that the critical crystalline size increases with increasing yttria contents. The presence of an external stress reduces the critical crystalline size at a given level of yttria content. Below the critical crystalline size, ZrO_2 is stable in the tetragonal form, but it can transform to monoclinic under stress-free conditions when the crystalline size exceeds the critical size (solid line). The critical size is reduced by an external stress, as shown in Fig. 7. For GTE/ZrO_2 nanocomposites studied, the sizes of the ZrO_2 nanoparticles are below the critical sizes required for the phase transformation to occur. Thus, the tetragonal-to-monoclinic transformation is energetically unfavorable; hence, the absence of transformation toughening in the ZrO_2-filled nanocomposites can be understood on the basis that the tetragonal ZrO_2 nanoparticles are overly stabilized. To induce transformation toughening, the size of the ZrO_2 nanoparticles must be increased or the yttria content must be decreased to just below the critical size boundary (solid line) so that the tetragonal-to-monoclinic transformation can occur under the assistance of an external stress.

Conclusions

The conclusions reached, based on the results of this investigation, are as follows:

1. ZrO_2 nanoparticles increased the fracture toughness of the nanocomposites compared to the matrix alone and those containing silica-nanoparticle fillers.
2. The fracture mechanisms in GTE/ZrO_2 nanocomposites include crack deflection by particles and fracture along the matrix/particle interface.
3. Transformation toughening is absent in nanoparticle-filled GTE because the ZrO_2 nanoparticles favor the tetragonal structure in the ranges of particle sizes and yttria contents examined. The particle size needs to be increased to induce transformation toughening.
4. The fracture toughness in GTE/ZrO_2 nanocomposites originates from the interface toughness, crack deflection, and a higher inherent fracture toughness of the ZrO_2 nanoparticles as compared to silica nanoparticles.

Acknowledgements This work was supported by National Institutes of Health through Grant No. P01DE11688. Technical assistance by Mr. D. E. Moravits, Southwest Research Institute (SwRI), in fracture testing and clerical assistance by Ms. A. Matthews and Ms. L. Mesa, SwRI, in the preparation of this manuscript is acknowledged.

References

1. Furman B, Rawls HR, Wellinghoff ST, Dixon H, Nicolella D (2000) Crit Rev Biomed Eng 28:439
2. Rawls HR, Furman B, Wellinghoff ST, Nicolella D, Dixon H, Ong JL, Park Y-J, Norling GK (2000) J Korean Res Soc Dent Mater 27:3
3. Park Y-J, Chae K-H, Rawls HR (1999) Dent Mater 15:120
4. Chan DCN, Titus HW, Chung KH, Dixon H, Wellinghoff ST, Rawls HR (1999) Dent Mater 15:219
5. Rawls HR, Wellinghoff VT, Norling BK, Leamon SH, Swynnerton NF, Wellinghoff ST (1997) ACS Polym Prepr 38(2):167
6. Wellinghoff ST, Dixon H, Nicolella DP, Norling BK, Rawls HR (1998) Metal oxide nanoparticle-polymer composites: structure property relationships, dental, and other applications. In: Fine, ultrafine and nano powders. Business Communication, Norwalk
7. Schulz H, Madler L, Pratsinis SE, Burtscher P, Mozner N (2005) Adv Funct Mater 15(5):830
8. Schulz H, Pratsinis SE, Rüegger H, Zimmermann J, Klapdohr S, Salz U (2008) Colloid Surf A 315:79. doi:10.1016/j.colsurfa.2007.07.016
9. Chan KS, Nicolella DP, Furman BR, Lee Y-D, Wellinghoff S, Rawls R (2007) Eng Fract Mech 74:1857
10. Bravo-Leon A, Morikawa Y, Kawahara M, Mayo MJ (2000) Acta Mater 50:4555
11. Lange FF (1982) J Mater Sci 17:240. doi:10.1007/BF00809059
12. Evans AG, Cannon RM (1986) Acta Metall 34(5):761
13. McMeeking RM, Evans AG (1982) J Am Ceram Soc 65:242
14. Zeng D, Katsube N, Soboyejo WO (2004) Mech Mater 36:1057
15. Mueller R, Jossen R, Pratsinis SE, Watson M, Akhtar MK (2004) J Am Ceram Soc 87:197
16. Jossen R, Mueller R, Pratsinis SE, Watson M, Akhtar MK (2005) Nanotechnology 16:S609
17. ASTM E399-90 (1999) Annual book of ASTM standards, vol 03.01. ASTM, West Conshohocken, p 422
18. Jossen R, Heine MC, Pratsinis SE, Akhtar MK (2006) CVD J 12:614
19. Faber KT, Evans AG (1983) Acta Metall 31:565
20. Liu AF (2005) Mechanics and mechanisms of fracture: an introduction. ASM International, Materials Park, p 298
21. Matsumoto RLK (1987) J Am Ceram Soc 70(12):C-366
22. Suresh A, Mayo MJ, Porter WD (2003) J Mater Res 18:2912
23. Joint Committee on Powder Diffraction Files, International Center for Diffraction Data, Swarthmore, PA, 1992